HOSTED BY
ELSEVIER
Available online at www.sciencedirect.com
ScienceDirect
Soils and Foundations 61 (2021) 386–400
SOILS AND FOUNDATIONS
www.elsevier.com/locate/sandf

Technical Paper

Vibration of subgrade and evaluation of derailment coefficient of train under combined earthquake- moving train load

M. Gao [a,*], X. Xu [a], R. He [b,c], Q.S. Chen [d], D.Y. Li [a]

[a] *Shandong Province Key Laboratory of Civil Engineering & Disaster Prevention and Mitigation (College of Civil Engineering and Architecture), Shandong University of Science and Technology, Qingdao 266590, China*
[b] *Key Laboratory of Coastal Disaster and Defense (Hohai University), Ministry of Education, Nanjing 210017, China*
[c] *College of Harbor, Coastal and Oshore Engineering, Hohai University, Nanjing 210024, China*
[d] *Department of Civil and Environmental Engineering, National University of Singapore, No.21 Lower Kent Ridge Road, 119077, Singapore*

Received 12 February 2020; received in revised form 17 December 2020; accepted 26 December 2020
Available online 3 February 2021

Abstract

Vibration response of track and foundation subjected to dynamic loading is one of the key issues to solve on-track safety of high-speed train. The previous pioneering works commonly only considered the train moving load, however, in reality, trains are likely to be on track when an earthquake occurs due to the high frequency and widespread distribution of earthquake activities. Hence, a three-dimensional FEM of track-subgrade- foundation interaction system with bidirectional seismic and moving loads is established for investigating the differences and relations of vibration responses of subgrade in such two immensely disparate loads: train moving load and earthquake-moving load. As a case study, the vibration characteristics of the Beijing-Shanghai High-speed Railway of the China, excited by moving load and seismic-moving composite load are analyzed respectively, with various velocity (v = 50 m/s, 70 m/s, 100 m/s, 130 m/s). On the other hand, the increases in operational train speeds mean that critical velocity effects are becoming more common on high speed rail lines. If unaddressed, critical velocity issues can cause safety concerns and elevated maintenance costs. Based on the derailment coefficient and lateral deformation of the rail, the critical speed of the model is discussed, which is a reasonable improvement to the derailment mechanism of the train.

Keywords: Bidirectional earthquake load; Moving train load; Vibration response; Critical speed; Derailment coefficient

1. Introduction

In recent decades, high-speed trains have been a major mode of public transportation. However, since the high-speed railway network occupies a considerable proportion in such earthquake-prone areas, the possibility that earthquakes will occur when trains are running is higher than ever before. For example, the 1976 Tangshan earthquake in China and the 2004 Niigata earthquake in Japan caused serious derailment accidents (see the Fig. 1). Taiwan's Kaohsiung earthquake with a magnitude of 6.7 derailed Taiwan's high-speed rail on March 5, 2010. Passengers described it as like riding a roller coaster, bumping and jumping all the way. Since the lateral force between wheel and rail is proportional to the square of the train speed (Schnellboegl, 2009), even the earthquake with lower magnitude may cause a major safety accident of derailment or even rollover when the speed exceeds 200 km/h. Therefore,

* Corresponding author at: College of Civil Engineering and Architecture, Shandong University of Science and Technology, Qingdao 266590, China.
E-mail address: gmxyz@sdust.edu.cn (M. Gao).

https://doi.org/10.1016/j.sandf.2020.12.005
0038-0806/

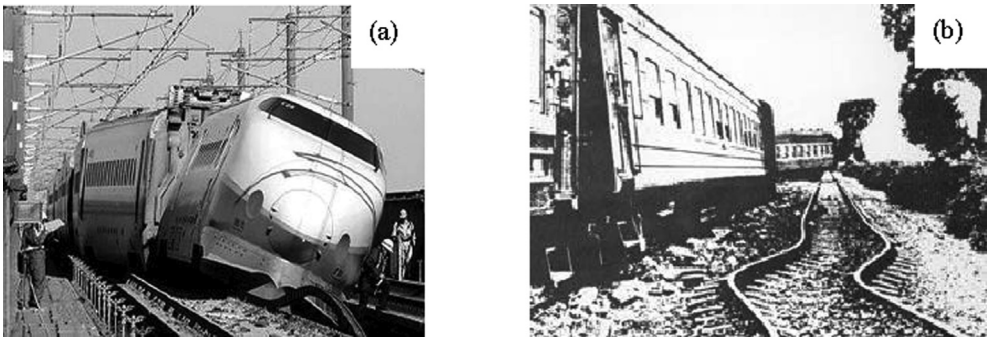

Fig. 1. Cases of train derailment caused by earthquake (a) Shinkansen Train Derailment Caused by Japan's Niigata Earthquake (b) Train derailment due to Tangshan Earthquake in China.

it is of great engineering value to study the seismic evaluation of the dynamic site of on-track high-speed trains.

As the safety, comfort and stability demands of moving high speed trains improve, the problem of ground vibration induced by moving train load has attracted a lot of attention. Takemiya, Hirokazu1 (2003), Paolucci et al.(2003) and Bian et al.(2008) attempted to demonstrate an application of the numerical simulation model for predicting the train-track and nearby ground-borne vibrations by the Swedish high-speed train X-2000 at Ledsgard. Cai et al. (2008a, 2008b) investigated the dynamic responses of a track system and poroelastic half-space soil medium under different train moving load patterns by the substructure method. By means of numerical simulations, Beskou et al.(2016) and Ruiz et al. (2017) analyzed vehicle-induced flexible pavement responses and traffic-induced railway ground vibrations using commercial programs ANSYS and PLAXIS, respectively. Gao et al. (2018) presented an investigation of parameters of saturated soil on ground vibrations and excess pore water pressures induced by moving train loads. Treating the ground as a multilayered structure, Lefeuve-Mesgouez and Mesgouez (2012) and Yao et al. (2016) evaluate the dynamic responses of the subgrade due to high-speed trains by three-dimensional semi-analytical approach. In addition to these papers, many other reports have also been devoted to this subject (Sheng et al., 2004; Fang et al., 2018; Hung et al., 2013; Zhai et al., 2010). Nevertheless, in all the above studies, the influence generated by seismic load on the vibration propagation and attenuation of high-speed railway subgrade was not taken into account.

Actually, it should be noted that, the literatures dealing with the vibration characteristics in such two immensely disparate load combinations are limited, in contrast to the case of the single train load. Yau and Frýba (2007) investigated the vibrations of a suspension bridge caused by train loads and the vertical support motions due to earthquakes. Tanabe et al. (2008) proposed a simple and efficient numerical method to solve the dynamic interaction of a high-speed train and railway structure during an earthquake. Zhang et al. (2010) performed a method to simulate the train-bridge interaction system under multi-support seismic excitations. Zeng et al. (2015) investigated the random vibrations of a high-speed train traversing a continuous girder bridge subjected to traveling seismic waves by the pseudo excitation method. Unfortunately, these pioneering works are investigated from the point of view of the interaction dynamics of the train-track/bridge system during earthquakes, with limited attention to the vibration characteristics of subgrade in moving-seismic joint action conditions.

It is found that, in all the above studies, most researchers either neglected the subgrade system or took only the moving load into consideration. The existing literature seldom discuss the vibration responses of the subgrade under combined moving loads and seismic loads. Thus, it would be of great importance for investigating the changes of dynamic responses of the subgrade structure due to the combined loads. Furthermore, in addition to the laboratory tests (Zhuang et al., 2016; Wang et al., 2016) and field investigations (Feng et al., 2017; Gao et al., 2017; Gao et al., 2015), numerical simulation is becoming a promising alternative to evaluate and analyze the geotechnical behavior of railway track to aid decision making in terms of technical and economic feasibility.

In view of this, this study establishes a 3D FEM of track- subgrade- foundation interaction system with bidirectional seismic and moving loads. The Beijing-Shanghai High-speed Railway in China is chosen to study wave motions generated in ground, since unique response features were observed during its operations. Seismic waves are selected from the real data of American Imperial Valley earthquake and input from the bottom of the model in two directions. Subsequently, the proposed approach is verified with the analytical and numerical solutions of an elastic homogeneous half-space subjected to a moving point load. The train speed as a significant factor on the dynamic responses is taken into consideration by modeling practical example in this note. With the aid of computer simulation, the mechanisms of vibration generation and propagation were interpreted. Finally, based on the derailment coefficient and lateral deformation of the rail, the critical speed of the model is discussed, which is a reasonable improvement to the derailment mechanism.

2. Model and parameters

2.1. Model design

As shown in Fig. 2, according to the *Code for Design of High Speed Railway* in China (Ministry of Railways of China, TB 10621–2009), a comprehensive track-subgrade-foundation system is established. The dimension of calculation model is determined by trial calculation. As the dimension of calculation model is doubled, the displacement is only increased by 10^{-6}m, which shows that the result of this calculation is convergent. The longitudinal length of the model along the route is 520 m, the width of the foundation surface is 52 m, and the total height is 27.706 m. The standard rail of 60 kg·m^{-1} is adopted, with a gauge of 1.435 m and a fastener fulcrum spacing of 0.65 m. As shown in Fig. 2, the upper track system consists of the rail, precast concrete rail plate, cement emulsified asphalt adjustment layer (CA mortar layer) and concrete base plate. The subgrade system is composed of three parts, namely, surface layer of subgrade, bottom layer of subgrade and subgrade ontology. In Fig. 3 and Fig. 4, the track systems are connected by linear springs and viscous damping, K and C are equivalent stiffness and damping coefficient of springs (Du et al., 2014; Song and Zhai, 2012). K_x and K_y are equivalent transverse and longitudinal stiffness of springs, respectively, and their values are all 37.5 kkN·m^{-1}. C_x and C_y are the transverse and longitudinal damping coefficients of the spring, both of which are 30 kN·m^{-1}. K_z and C_z are equivalent vertical stiffness and damping coefficient of spring, which are 25kN·m^{-1} and 37.5kN·m^{-1}, respectively.

The FE dynamic analysis model of the track structure - subgrade - foundation is built by ABAQUS (Abaqus 6.14 Getting Started with Abaqus Interactive Edition). The number of nodes in the whole model is 801,629 and the number of units is 648,000. The established model is shown in Fig. 5, each component of the calculation model adopts an elastic constitution The three-dimensional viscoelastic artificial boundary can well simulate the real situation of wave propagation through the boundary facing semi-infinite medium, and can obtain the calculation result with the same accuracy as the far boundary condition. Therefore, as shown in Fig. 6, the viscoelastic boundary is

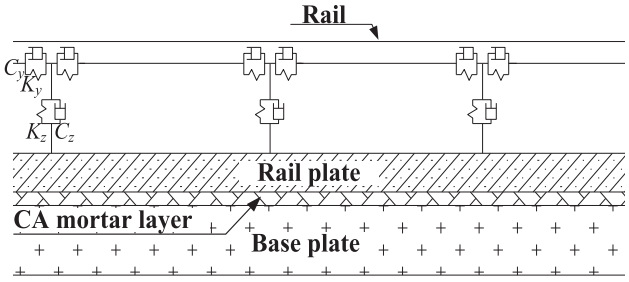

Fig. 3. Side view of model of slab ballastless track.

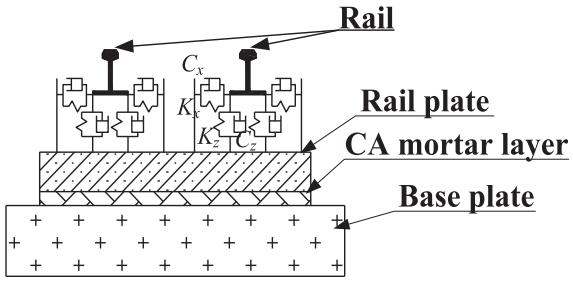

Fig. 4. End view of model of slab ballastless track.

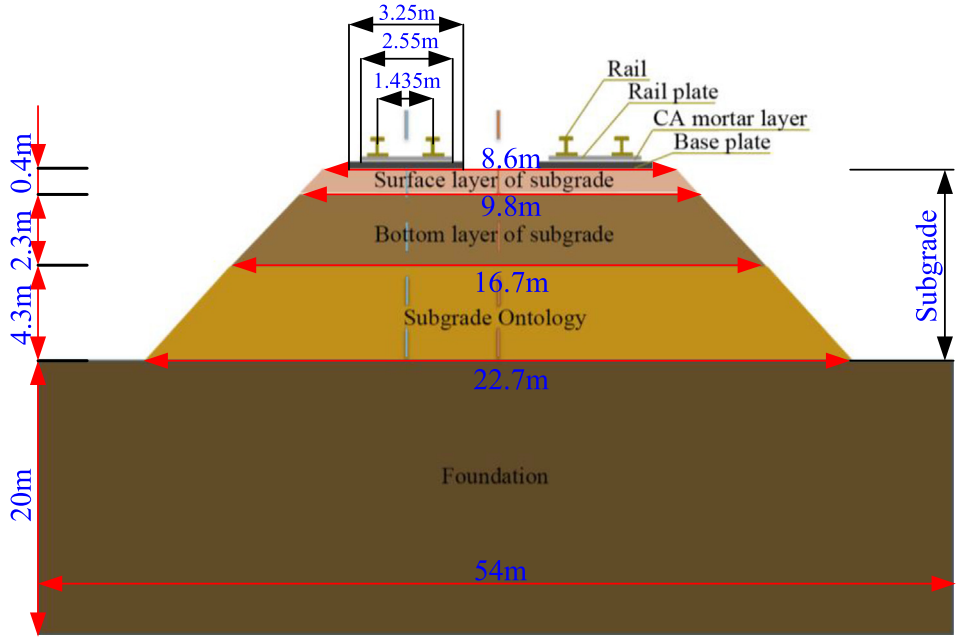

Fig. 2. Profile of calculation model.

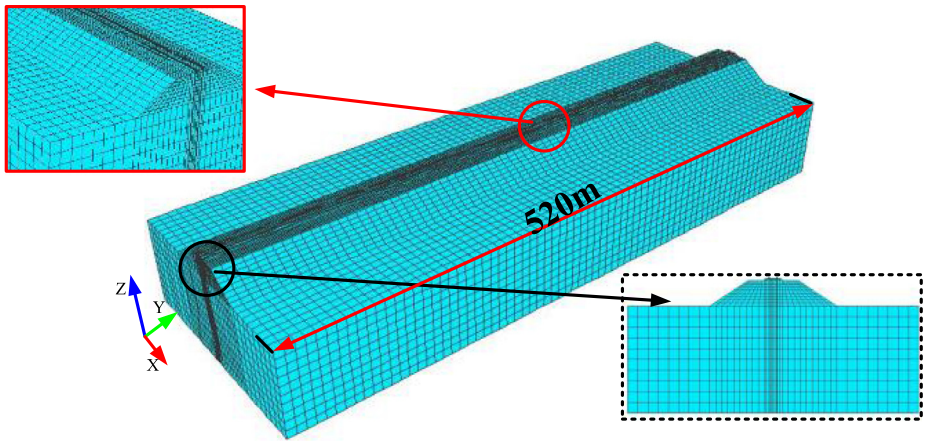

Fig. 5. Finite element computing model.

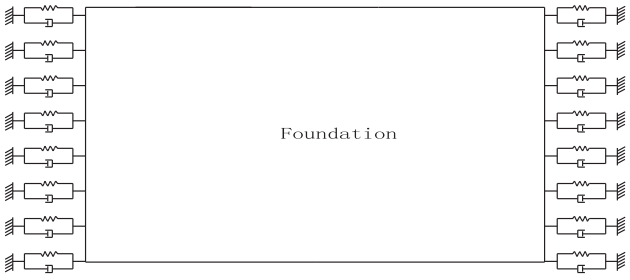

Fig. 6. Schematic diagram of viscoelastic boundary conditions.

adopted at four sides of the foundation, and fixed boundary condition is adopted at the bottom to simulate wave propagation from finite domain to infinite domain. As the sliding between the rail plate and the surface of subgrade, the subgrade ontology and the foundation is relatively small, contact pairs (i.e. Tie contract) are applied to simulate the dynamic interaction so as to keep the deformation coordination between the contact surfaces, which does not restrict the rotational freedom of the corresponding nodes on the two surfaces. The basic physical and mechanical parameters of each soil layer and structural layer of ballastless track of high-speed railway come from Chinese Code for Design of High-speed Railway, the selection of damping coefficient comes from Du et al. (2014), and the selection of damping ratio comes from Xue et al (2014). The material parameters of the elements used in FE dynamic analysis are shown in Table 1.

2.2. Moving load

The train dynamic load on the track during train operation includes three parts: moving dynamic load, fixed point dynamic load and moving axle load (Yuan et al., 2016). The main purpose is to study the dynamic response of subgrade, so the influence of wheel-rail contact irregularity is ignored. The vertical load of train will be taken into account during simulation. The model selects the most unfavorable multi-axis excitation form, that is, four wheels of end bogies of two adjacent vehicles, to analyze the dynamic performance of subgrade. Through secondary development, the subroutine DLOAD is compiled and combined with ABAQUS program to realize the application of train load. In the model, the running direction of moving load (i.e., Y axis) is taken as the positive direction, and the running speed v and time t of the train are selected to define the moving coordinate of the load, i.e., $y = y_0 + vt$, where y_0 is the initial coordinate value of the wheel load. The wheel-rail contact is surface contact, so the axle load of train axle is set as the moving surface load applied on the rail surface, and the action range of the wheel-rail contact point is set as 0.05 m × 0.02 m.

Fig. 7 shows a train consisting of a series of four-wheelset vehicles moving at a constant speed v on a rail structure. The CRH3 EMU (Sun et al., 2014) is selected as the train load with a length of about 200 m. The length of the intermediate vehicle is 25 m and the fixed distance of train is 17.375 m. The fixed wheelbase of the bogie is 2.5 m, the wheelbase between the two trains is 4.5 m and an axle load of 17 t.

2.3. Earthquake load

Seismic intensity indicates the degree of damage caused by earthquake to the ground surface and engineering structure. According to the corresponding table of seismic fortification intensity and peak acceleration value of ground motion in *Chinese Code for Seismic Design of Railway Engineering* (Ministry of Construction of China, GB 50111–2009) (i.e. Table 2), intensity of 7 degrees indicates that the structure has entered an elastoplastic state. As shown in Fig. 8, therefore, two horizontal acceleration time-history data of the Imperial Valley seismic wave from Joyner and Boore (1981) are selected, and the peak value of the seismic wave is adjusted to 0.1 g. Take the acceleration

Table 1
Parameters of the finite element computing model.

Name	Thickness (m)	Density (kg/m^3)	Elastic modulus (GPa)	Poisson's ratio (v)	Damping ratio ζ	Rayleigh damping coefficient	
						α	β
Rail	0.176	7800	210	0.3	0.01	0.14488	0.00069
Rail plate	0.2	2500	35.5	0.2	0.03	0.43453	0.00207
CA mortar layer	0.03	1800	7.0	0.2	0.05	0.72439	0.00345
Base plate	0.3	2500	30	0.2	0.03	0.43453	0.00207
Surface layer of subgrade	0.4	1950	0.25	0.3	0.08	1.15902	0.00552
Bottom layer of subgrade	2.3	1900	0.2	0.25	0.07	1.01414	0.00483
Subgrade ontology	4.3	1850	0.15	0.25	0.10	1.44878	0.00690
Foundation	20	1800	0.1	0.25	0.08	1.15902	0.00550

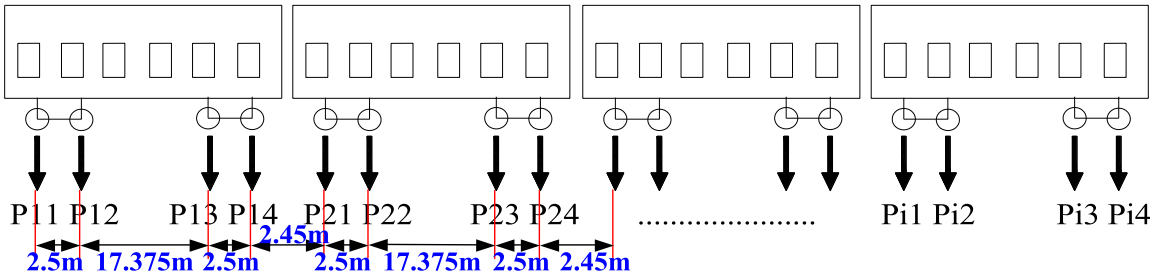

Fig. 7. Profile of train wheel-axel loads.

Table 2
Seismic fortification intensity and earthquake peak acceleration value.

Seismic fortification intensity	6	7		8		9
Seismic peak acceleration value	0.05 g	0.10 g	0.15 g	0.20 g	0.30 g	0.40 g

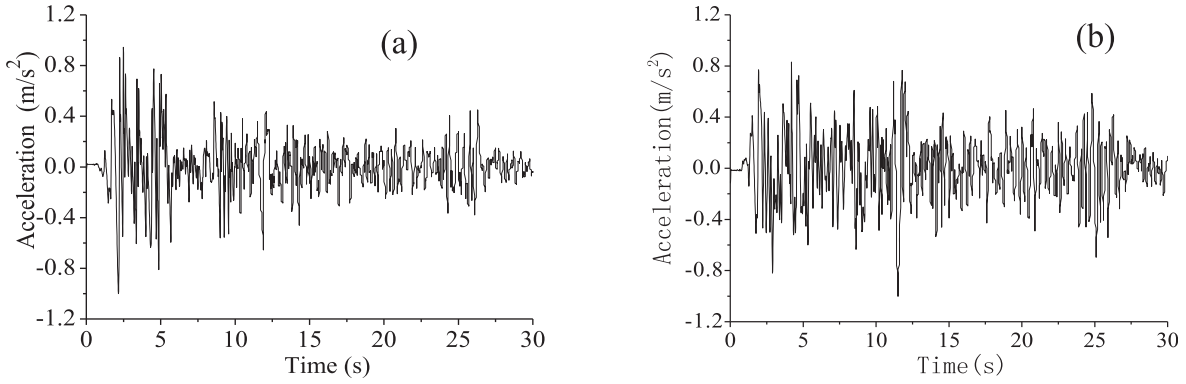

Fig. 8. Acceleration time history of Imperial Valley (a) Seismic acceleration in horizontal H_1 direction (b) Seismic acceleration in horizontal H_2 direction.

of 2 ~ 3.6 s during the strongest seismic intensity period, and input from the bottom of the model.

3. Verification of model effectiveness

In this section, the verification of the 3D FEM for elastic medium is carried out. The upper track structure in the three-dimensional numerical model is simplified to a Euler beam in Fig. 9. The dimension (X, Y, Z) of the model is 52 × 520 × 20(m × m × m). The width of the beam is B = 3 m, the bending rigidity EI = 13.254MN·m^2, and the mass m = 540 kg/m. In the verification, the moving point load travels in positive Y-direction. The density of the soil is 2000 kg/m^3, the shear-wave velocity is 100 m/s, Poisson's ratio is 0.25, the damping ratio is 0.05. The boundary conditions of the model are shown in the Fig. 6.

The dynamic responses at 1.0 m beneath the ground surface due to a moving point load with the speed of 60 m/s are investigated. The normalized displacements of longitudinal and vertical responses multiplying $2\pi\rho V_s^2/p$ are pre-

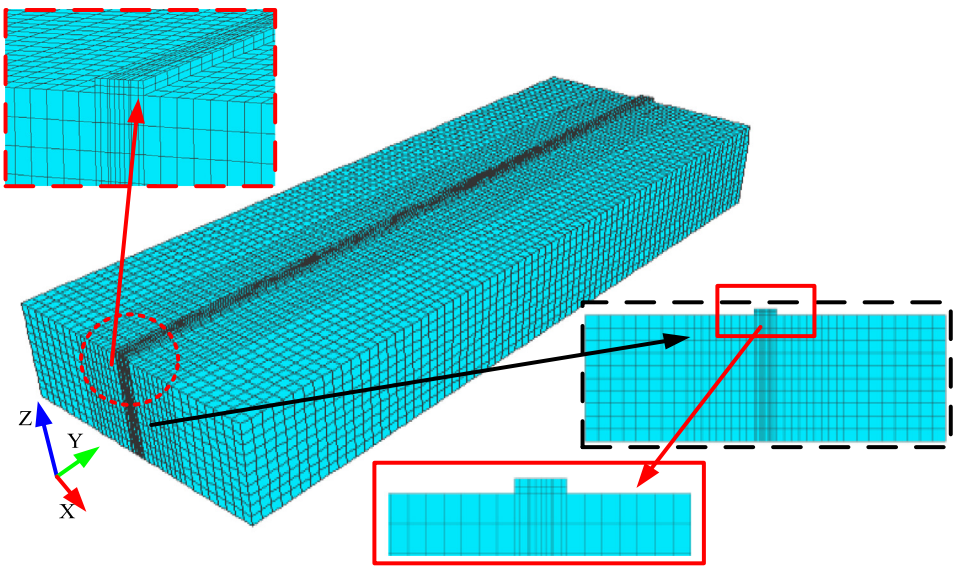

Fig. 9. Generated 3D Numerical Model.

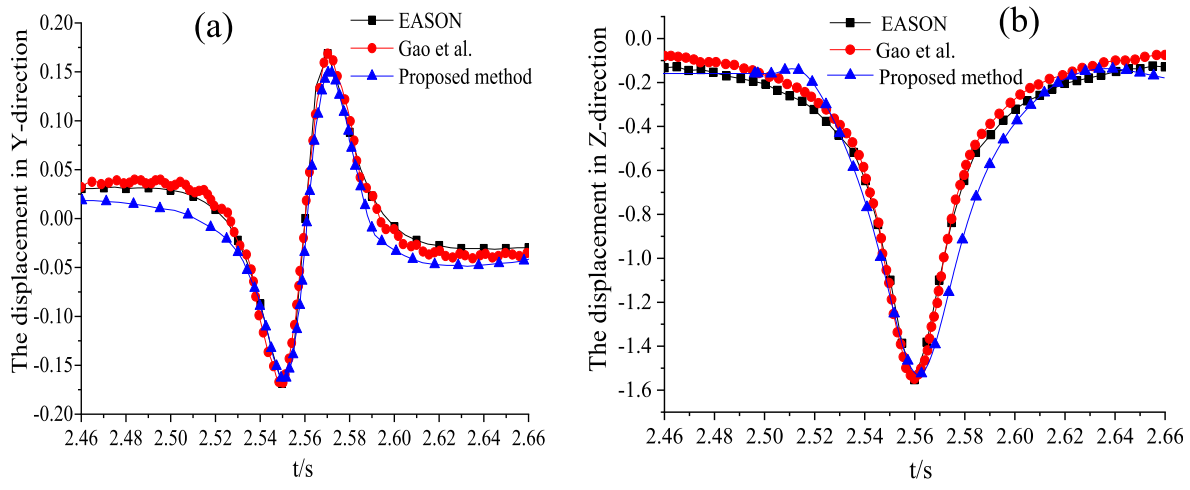

Fig. 10. Time histories of dynamic displacement for single wheel in subgrade surface (a) The displacement in Y-direction (b) The displacement in Z-direction.

sented in Fig. 10. In the same figure, the analytical solutions from the literature Eason (1965) and the 2.5D numerical solutions from the literature Gao et al. (2012) are also depicted for comparison. As shown in Fig. 10, the solutions by the present approach is in good agreement with those from the literature Eason (1965) and Gao et al. (2012).

4. Dynamic responses analysis under train-earthquake load

The high speed train not only has a more serious impact on people's life but also makes greater damages for railway structures than a normal-speed train does. Therefore, it is of great significance to study the vibration response laws of subgrade and rail structures at different speeds to ensure the safety and stability of high-speed railway operation. Considering the train speed index, the dynamic responses of subgrade (4.1) and train rail structure (4.2) due to the coupling effect of earthquake and moving load are respectively investigated in this section.

The track-subgrade- foundation system is established for investigating the differences and relations of vibration responses of subgrade in such two immensely disparate loads: train moving load and earthquake-moving load. Earthquake-moving load refers to only applying seismic waves in the first 1 s, and trains enter after 1 s, and the moving load and seismic load act together.

4.1. Vibration responses of subgrade

4.1.1. Subgrade dynamic displacement

Fig. 11 depicts the time history of vertical displacement of subgrade surface layer at different train speeds without applying earthquake load. It is observed that the change trend of the vertical displacement amplitude of the surface

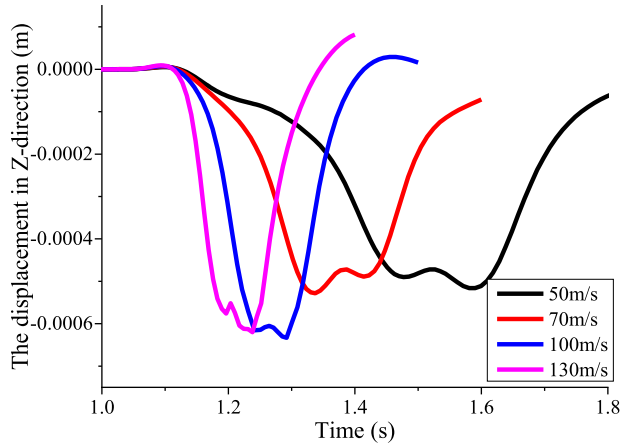

Fig. 11. Vertical dynamic displacement of top surface layer of subgrade at different speeds under moving load (0–1 s is the global convergence equilibrium time of the model).

layer of subgrade is basically the same at four different vehicle speeds, and the overall trend is increasing first and then decreasing. With the increase of vehicle speed, the displacement peak value gradually increases. When the moving train speed reaches 100 m/s, the maximum displacement of subgrade surface layer is 0.633 mm.

Fig. 12 depicts the time history of vertical displacement of surface layer of subgrade under earthquake load with various train speeds. Because the top surface of the model is a free boundary condition, the vertical displacement of the subgrade surface firstly shows a fluctuating upward trend and reaches a displacement peak of about 3 mm under the action of 0 ~ 1 s only earthquake load (that is, the train hasn't arrived yet). Then, the train drove in, the earthquake load and the moving train acted together, and the dynamic displacement of the subgrade surface greatly attenuated, decayed to 0, and increased reversely. Moreover, it is found that the four curves are closely distributed with little difference, and the maximum displacement variation is only 0.09 mm (every 10 m/s). That is,

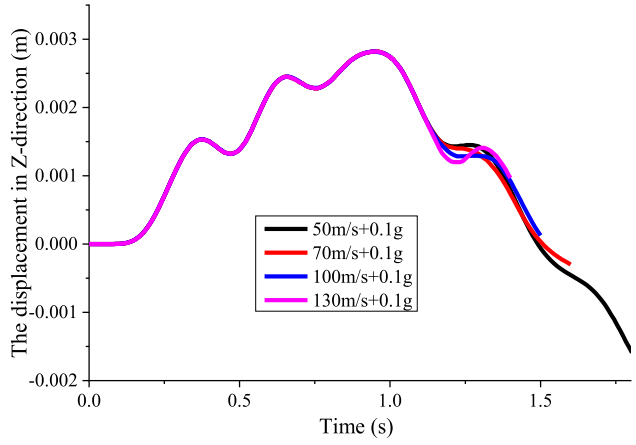

Fig. 12. Vertical dynamic displacement of top surface layer of subgrade at different speeds under composite load.

the operating speed has little effect on the vertical displacement amplitude of the subgrade surface. When the earthquake- moving load act together, the effect of earthquake load on the foundation bed is mainly shown. When earthquake-moving load is coupled, the influence of earthquake load on subgrade surface is dominant.

4.1.2. Subgrade acceleration and spectrum

Figs. 13 and 14 are acceleration time history and spectrum curves of subgrade surface when train speeds are 50 m/s, 70 m/s, 100 m/s and 130 m/s respectively. Figs. 15 and 16 show the acceleration time history and spectrum curves of subgrade surface under the moving-earthquake composed load.

It is observed from Fig. 13 that the peak acceleration of subgrade surface is the largest at 100 m/s, reaching 1.42 m/s. As can be seen from Fig. 14, under the action of a single moving train load, the dominant frequency of the subgrade surface layer is mainly maintained at medium–low frequencies, except for the vehicle speed of 100 m/s case. For the case of speed 100 m/s, the peak spectral acceleration is about 0.085 m/s^2, which is 2.5 times higher than that at other speeds, and its dominant frequency is 140–170 hz, with concentrated distribution, less energy propagation attenuation and large energy accumulation, which has adverse effects on train operation. That is, 100 m/s is close to the critical dangerous speed of the train. This result is consistent with the findings of Gao et al. (2012).

It is can be seen from Fig. 15, the acceleration is very sensitive to changes in moving train load. On the other hand, of course, it is also the most important that the vibration acceleration peaks are 2.52 m/s^2, 10.32 m/s^2, 4.80 m/s^2 and 2.92 m/s^2 respectively under the combination of 4 speeds and earthquake load, which are 5.1 times, 12.2 times, 3.37 times and 2.10 times of the corresponding accelerations in Fig. 13. Consequently, it shows that under the action of composite load, the acceleration amplitude changes dramatically for the case of the train speed 70 m/s (i.e. 250 km/h). It is presumed that the high-speed train shows certain vibration amplification effect at this speed.

As observed from Fig. 16 that the frequency corresponding to the peak value moves to the high frequency direction as a whole with the increase of train speed due to the earthquake-moving load. It is interesting to observe that the high frequency components of the spectrum curve at 50 m/s are much more severe than those at high speed (e.g. 100 m/s,130 m/s). Therefore, an appropriate increase in vehicle speed is conducive to the propagation and attenuation of medium–high frequency vibration energy. In addition, for the case of speed 70 m/s, the peak acceleration of frequency spectrum is about 1.58 m/s^2, which is 7.9 times higher than other running speeds. What is more noteworthy is that the dominant frequency distribution is more concentrated at this speed, and the accumulated energy brings great potential dangers to the operation safety of

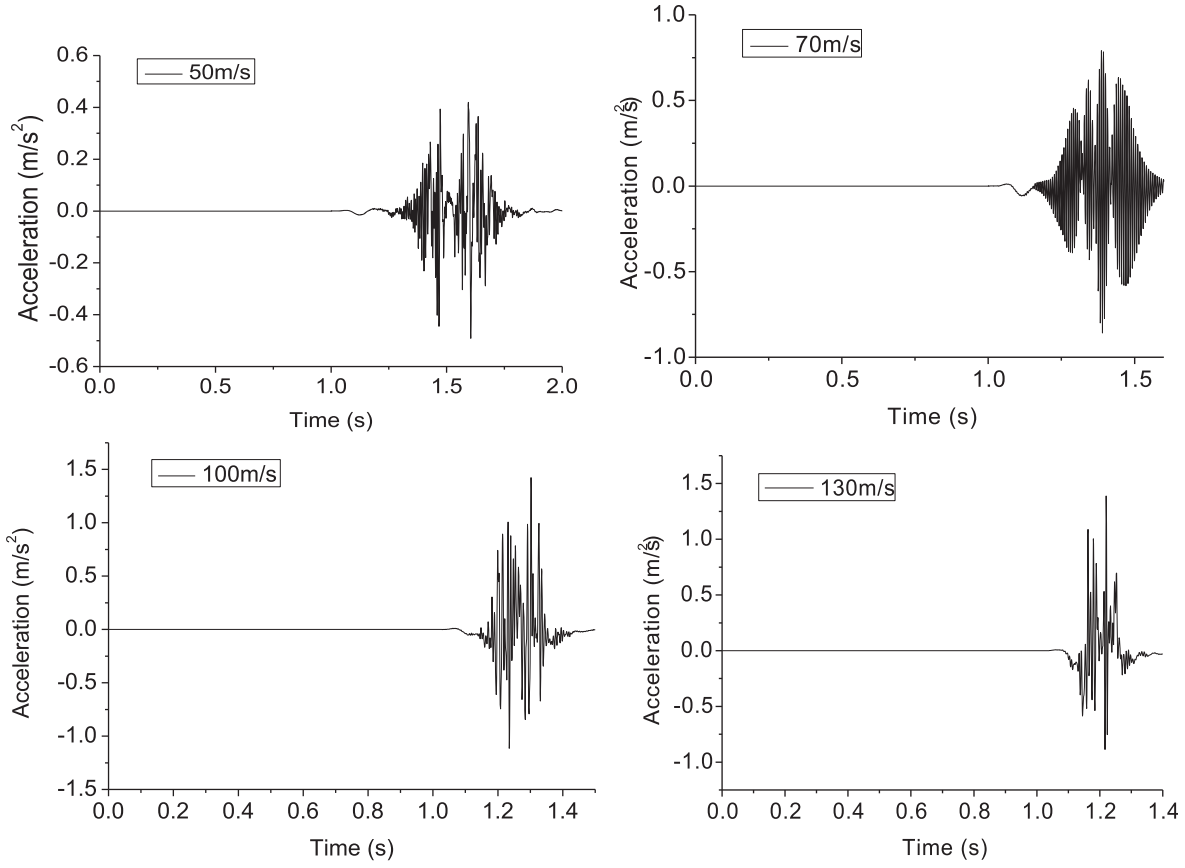

Fig. 13. Acceleration time history curve of moving load under different speeds.

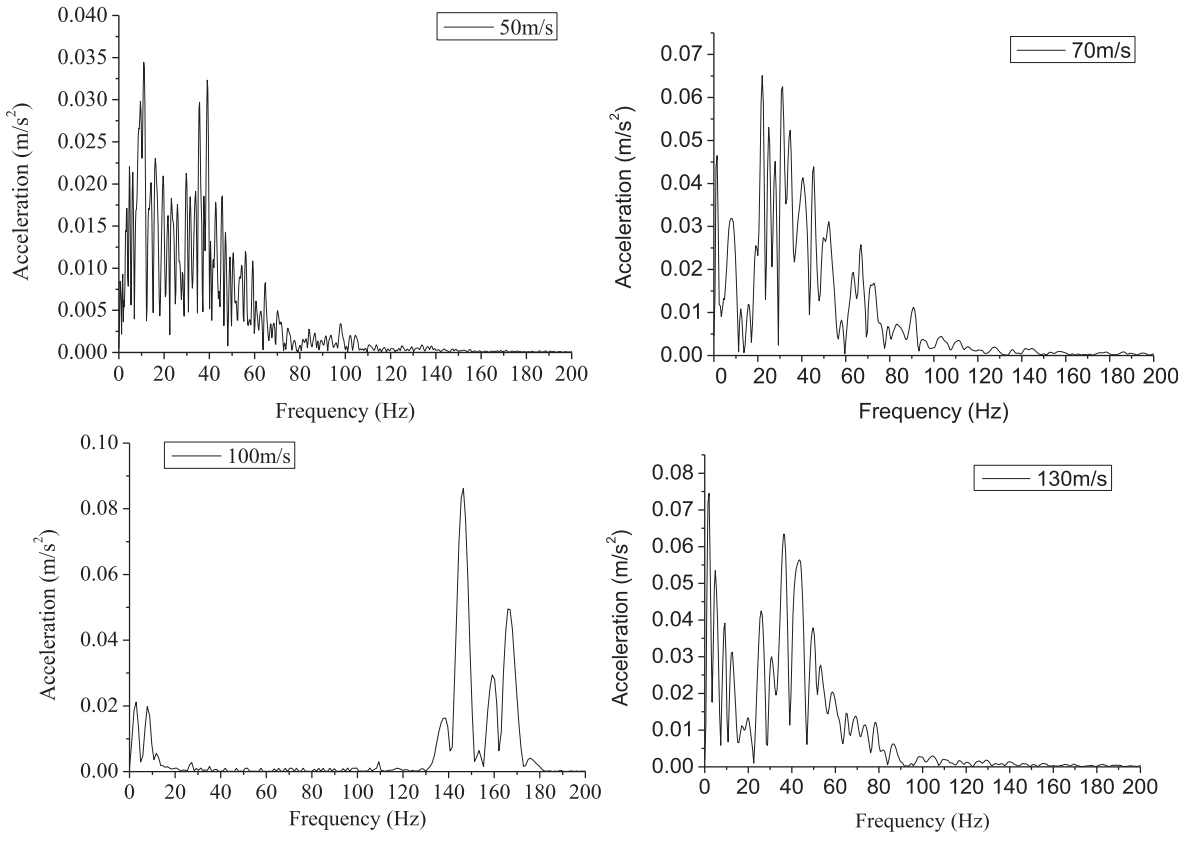

Fig. 14. Acceleration spectrum curve of moving load under different speeds.

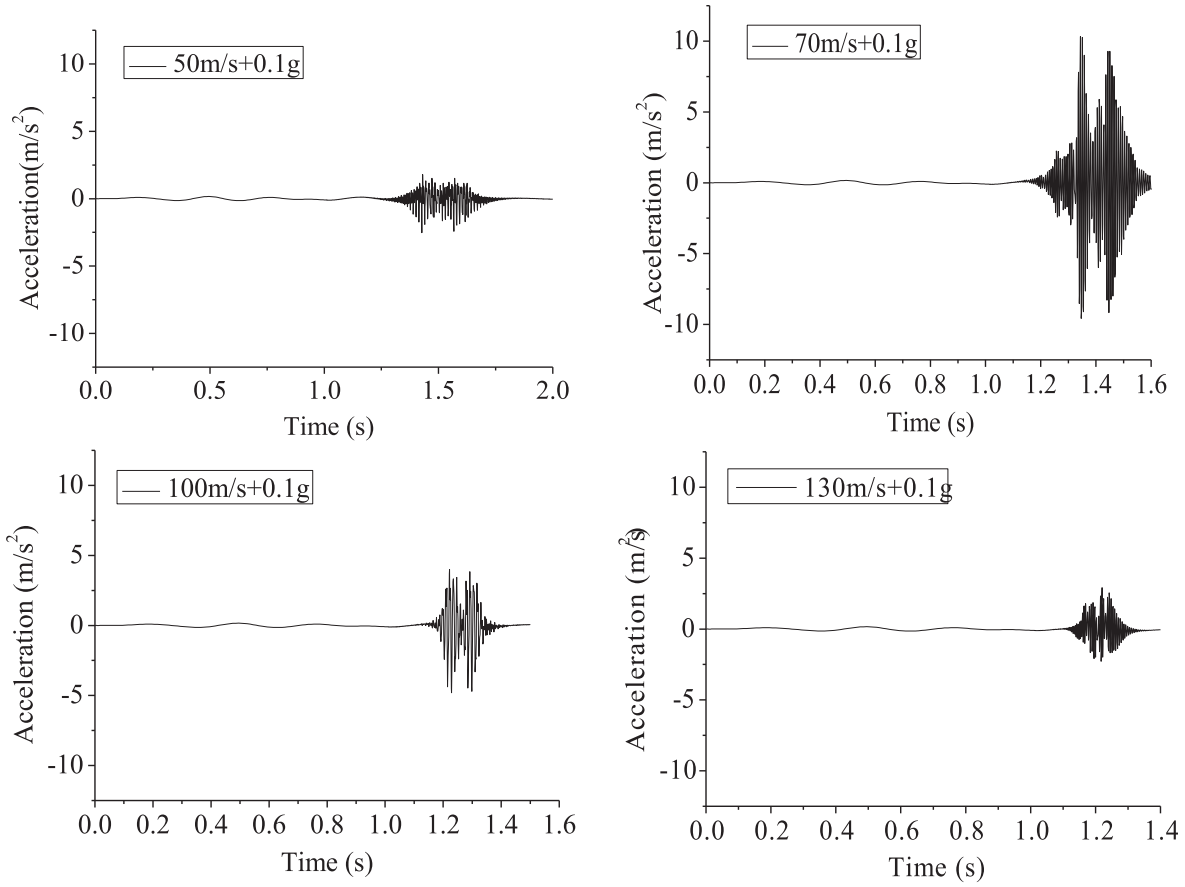

Fig. 15. Acceleration time history curve of composite load under different speeds.

high-speed railway. This phenomenon echoes the observations as shown in Fig. 15.

4.2. Vibration response of rail under earthquake - moving loads

4.2.1. Rail dynamic displacement

For the case of the speed of 70 m/s, as shown in Figs. 17–19, the impact of seismic load on rail displacement is illustrated. Therein, U_1, U_2 and U_3 respectively represent displacements in X, Y and Z directions. As observed, the rail displacement changes are mainly in X and Z directions, and the Y direction displacement changes are relatively small. Specifically, the application of seismic load increases the peak displacement of the rail in the X direction to 9.01 mm, which is about 25 times of the rail displacement under the action of only moving load. The composite load has little effect on the Y - direction displacement, but the increase is as high as 51.3% as compared with only moving load (Fig. 18(b)). For Z- direction displacement, the moving load generates negative displacement, and the seismic load generates positive displacement. Under the coupling effect of the two, the negative peak displacement of the rail raises slightly, while the positive peak displacement is about 652 times of the original (Fig. 19(b)), which is likely to cause the train to derail.

In order to further evaluate the influence of earthquake load on the vertical displacement of rail, Fig. 20 and Fig. 21 reveal the vertical vibration displacement curves of rail at different speeds, under the action of earthquake load or not. It is observed from Fig. 20 that the variation trend and peak amplitude of vertical displacement of rail are basically the same at different train speeds. The wheel-rail distribution of the train is relatively clear, which bear a stunning similarity to that for displacement nephogram (Fig. 19(b)).

It is noted from Fig. 21 that the dynamic amplitude of the rail fluctuated upward within 1 s due to the influence of earthquake load. After 1 s, the moving load is superimposed and dominated, and the rail displacement shows a decreasing trend as a whole. It is worth noting that the vertical displacement of the rail is not proportional to the running speed of the train. Under the earthquake moving load, the frequency of the seismic wave is nearly equal to the track frequency of the vibration caused by the moving train at the speed of 50 m/s (both 20 Hz), which will cause resonance. There is a critical speed of 50 m/s, at which time the rail displacement changes are the largest. Compared with the peak displacement reached at 1 s, the maximum change

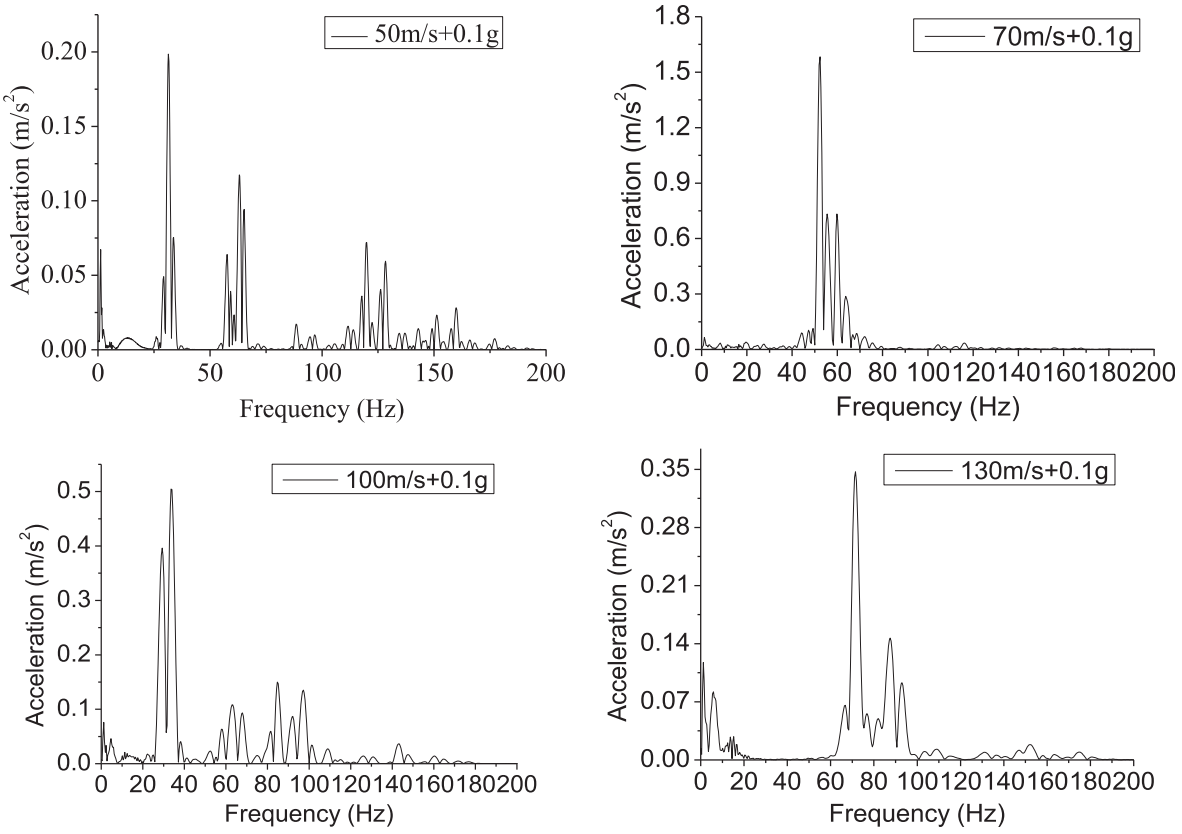

Fig. 16. Acceleration spectrum curve of composite load under different speeds.

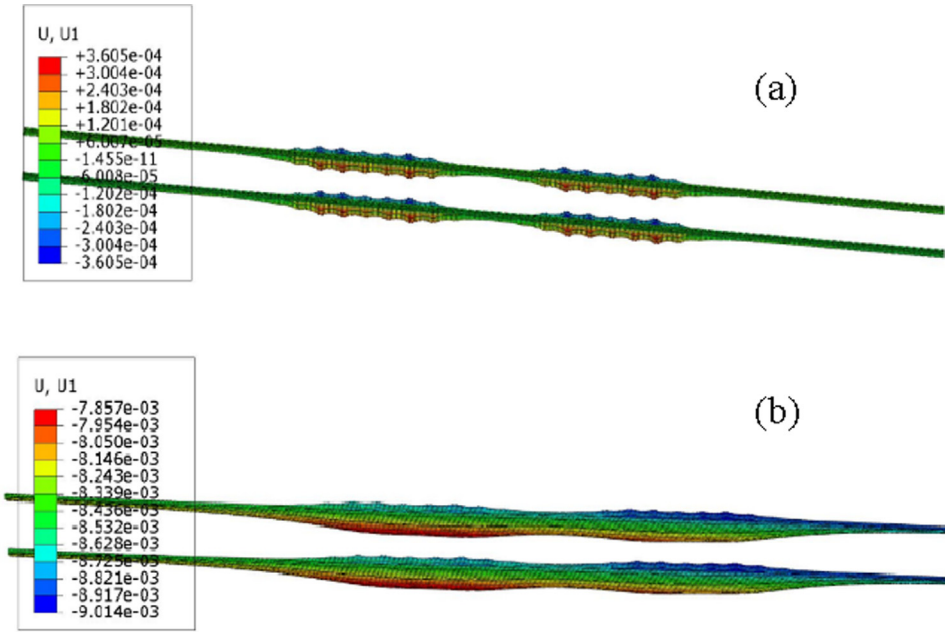

Fig. 17. X - direction displacement nephogram of rail (a) under moving load; (b) under composite loads.

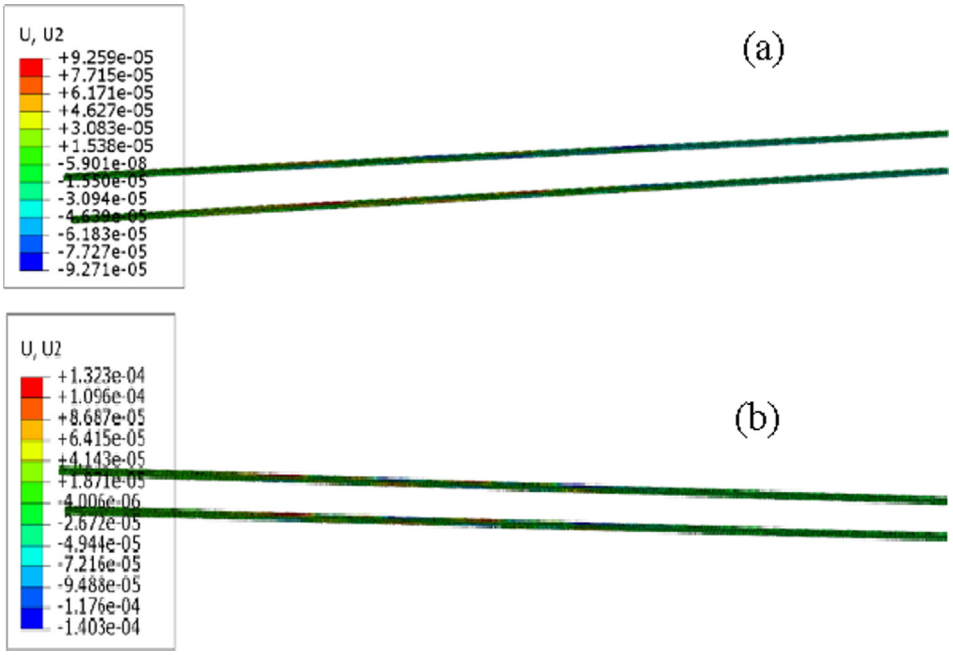

Fig. 18. Y - direction displacement nephogram of rail (a) under moving load; (b) under composite loads.

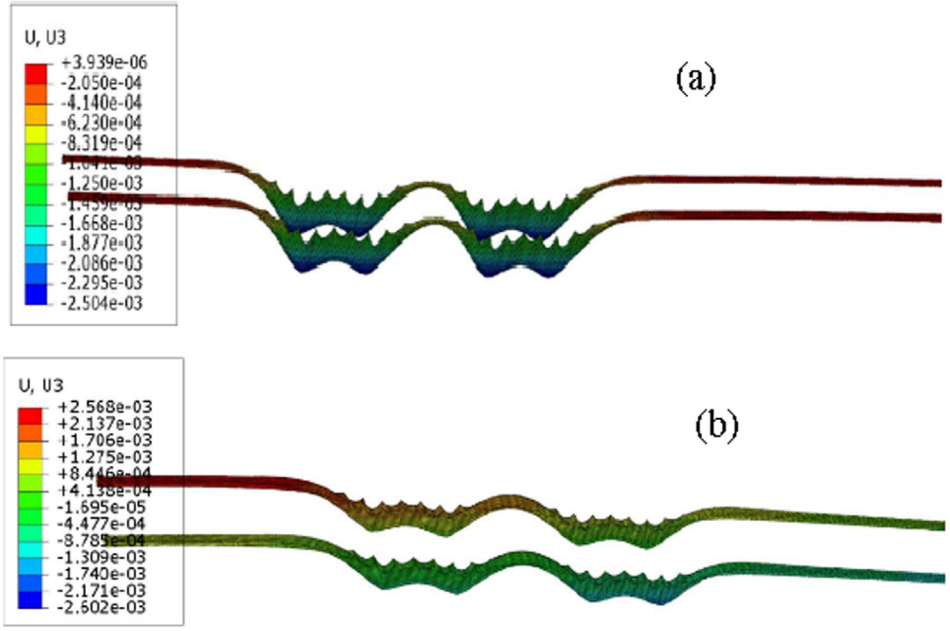

Fig. 19. Z - direction displacement nephogram of rail (a) under moving load; (b) under composite loads.

is about 4 mm, which is 1.6 times of the displacement changes at other speeds. At the critical speed, train moving loads induce strong vibration in track structure, and increase the risk of train derailing and track structure damage.

4.2.2. Derailment coefficient

To further investigate the relationship between earthquake load and train derailment mechanism under different operating speeds, the derailment coefficient safety standard: $Q/P \leq 1.2$ stipulated by the International Union of Railways(UIC) (Yi, 2018) is quoted. Where Q and P are the lateral force and the vertical force of the wheel and rail respectively. Their relationship to the lateral force and the vertical force of the track is the action and reaction, which they are equal in size and opposite in direction. The lateral force and vertical force of the track can be calculated by the finite element model established in this paper. With

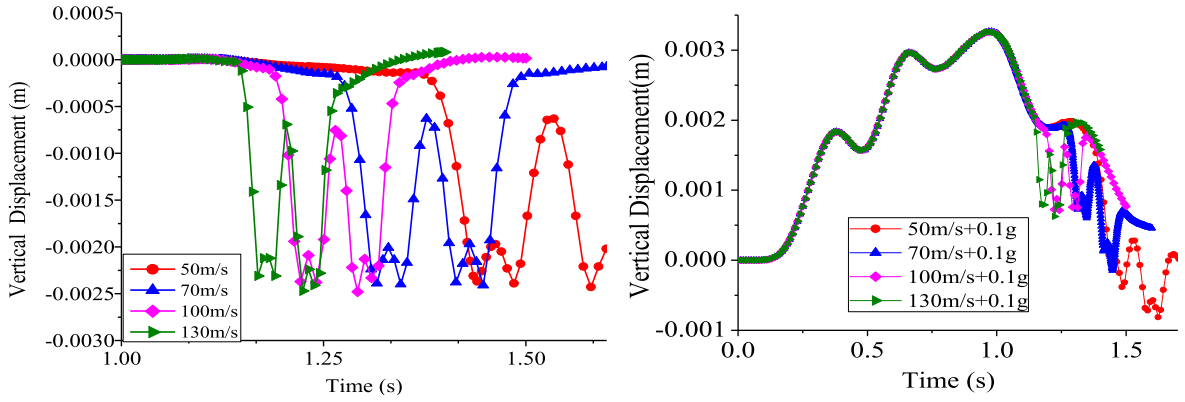

Fig. 20. Displacement curve of rail under moving load Fig. 18 Displacement curve of rail under composite load.

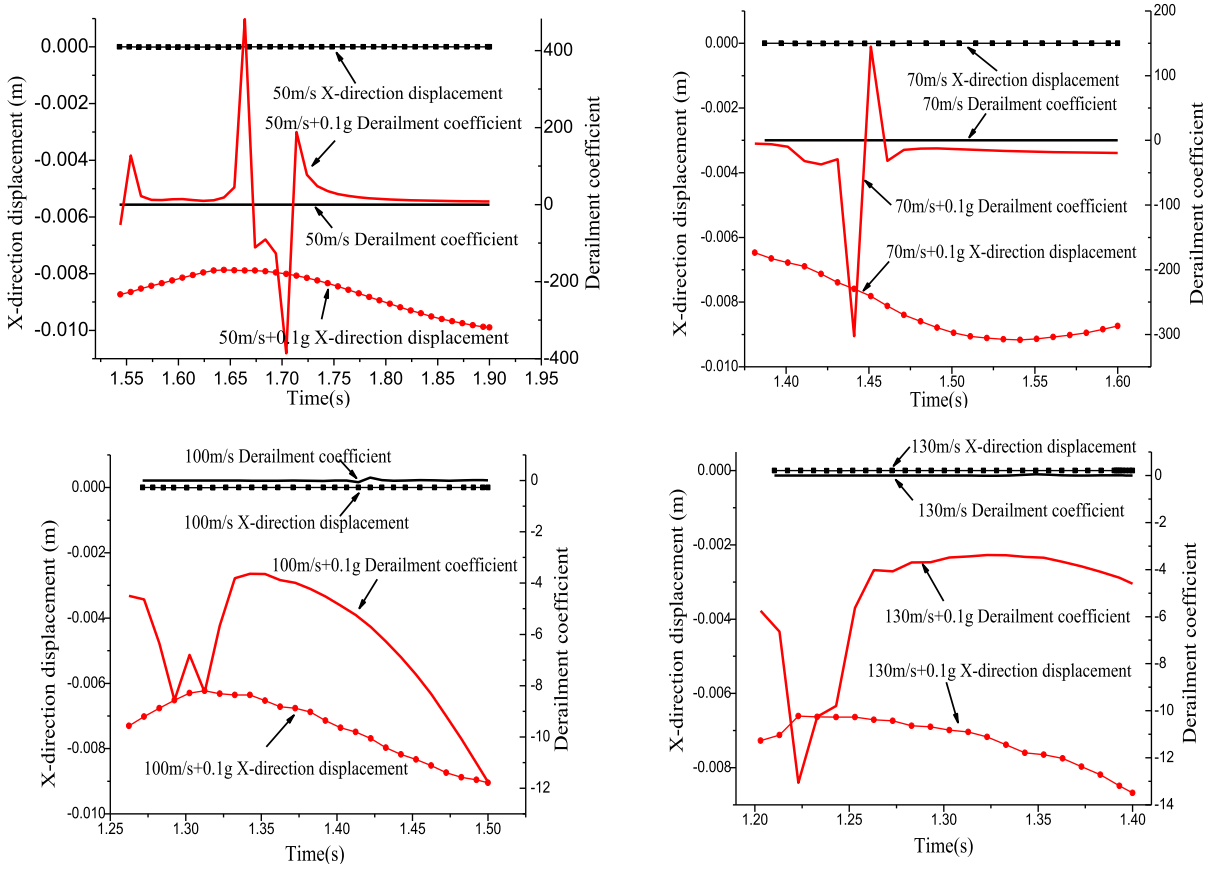

Fig. 21. Derailment coefficient curve under different train speeds.

or without earthquake load, the derailment coefficient and lateral displacement (i.e. X-direction displacement) of the rail at different speeds are plotted in Fig. 22.

It is observed from the Fig. 22 that the derailment coefficient and lateral displacement of the four kinds of running speeds due to no earthquake load fluctuates around 0. The lateral displacement is tiny in this context, the derailment coefficient meets the UIC code, and the train is in its secured state. This also proves that the current model has satisfying performance.

Under the joint action of earthquake and moving train, the lateral displacement increases significantly, and the derailment coefficient exceeds the safety standard. The observation shows the train derailment coefficient curve changes most dramatically at the running speed of 50 m/s and 70 m/s, that is, Derailment coefficient for 50 m/s and

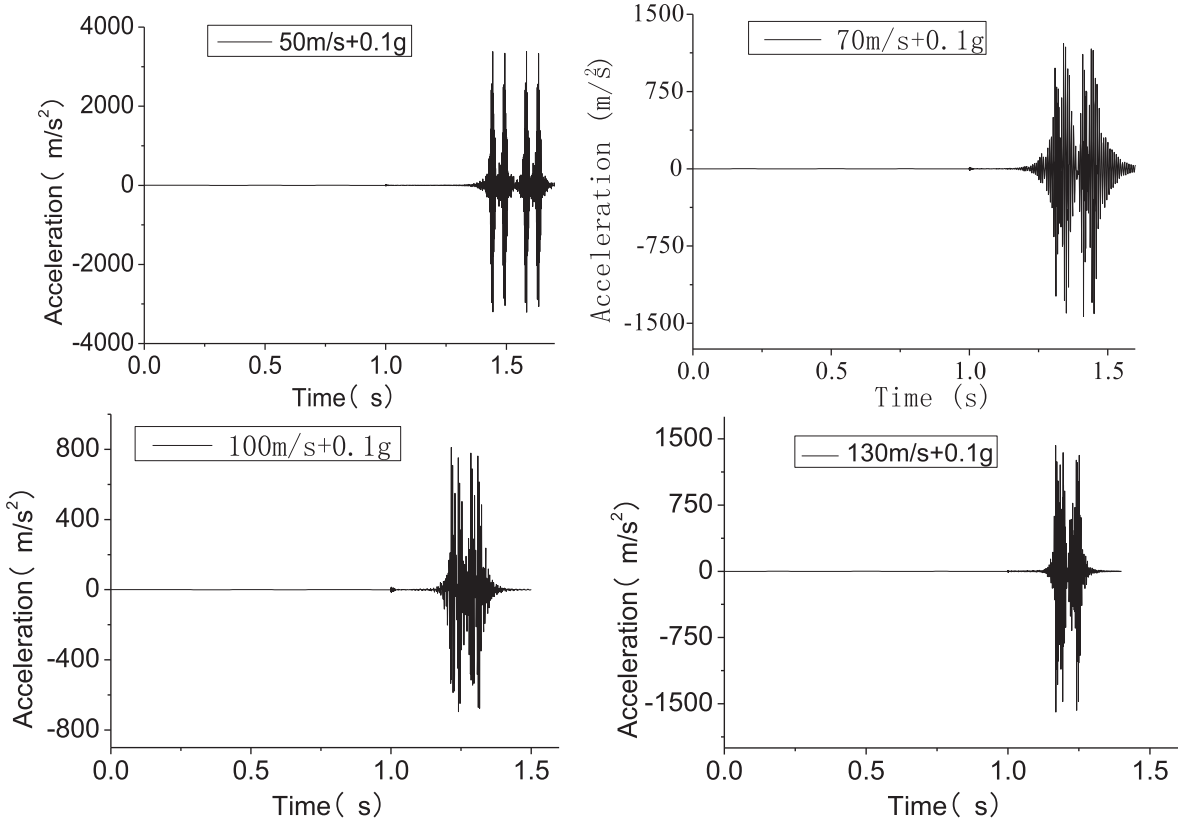

Fig. 22. Acceleration time history curve of composite load under different train speeds.

70 m/s is significantly larger than that of 100 m/s and 130 m/s. It is due to the fact that the frequency of the seismic wave is nearly equal to the track frequency of the vibration caused by the moving train at the speed of 50 m/s (both 20 Hz), while the moving train at the speed of 70 m/s, the track frequency of the vibration is close to the frequency of the foundation vibration (both about 30 Hz). Both will cause resonance, which will cause strong vibration of the track structure. Furthermore, the x-direction displacement of track caused by seismic load is much larger than that caused by moving load. Therefore, Derailment coefficient for 50 m/s is larger than that of 70 m/s. At the speed of 50 m/s, the lateral deformation suddenly reaches 8 mm at 1.66 s. As for the derailment coefficient, it is as high as about 500, seriously exceeding the safety limits of train operation. This finding is also consistent with the observation of the critical dangerous velocity of 50 m/s in Fig. 21. In addition, it is also observed that the abrupt point of lateral displacement of the track is basically coincided with that of derailment coefficient. Therefore, for the sake of safety, derailment coefficient and lateral displacement are taken as indexes to jointly serve as criteria for judging train derailment.

4.2.3. Rail acceleration and spectrum

Fig. 22 presents the acceleration time-history curve of rail at different operating speeds subjected to seismic load excitation. The acceleration time history fluctuates weakly within 0 ~ 1 s, i.e. the acceleration amplitude is not sensitive to the application of seismic load. Then, the train moving load with different running speeds is applied, and the acceleration of the rail fluctuates significantly. This phenomenon echoes the observations as shown in Fig. 15. It is noted from the observations of peak acceleration at different speeds that the vibration frequency of the rail is the fastest at 50 m/s (i.e. 180 km/h), and its acceleration reaches the maximum value of 338.405 g at about 1.44 s, which is 328 times of the peak acceleration of the subgrade. The literatures (Wang et al., 2016; Zhai et al., 2009) by Zhai WM team show that the acceleration of the rail is 190 ~ 225 g only under moving load. This can be explained by the fact that the rail structure, as a direct carrier, is remarkable. Meanwhile, due to the damping and filtering effects of soil layer, the vibration energy is transmitted to the subgrade and greatly attenuated.

Fig. 23 depicts the acceleration spectrum curve of the rail under the action of 0.1 g seismic acceleration and the moving load, with various operating speeds (v = 50 m/s, 70 m/s, 100 m/s and 130 m/s respectively). It is observed that the high frequency component of the rail structure is the main component in general. The composite loading with a speed of 50 m/s produces more focused and denser high-frequency components. This also indicates that 50 m/s is a dangerous speed of the train subjected to the moving-

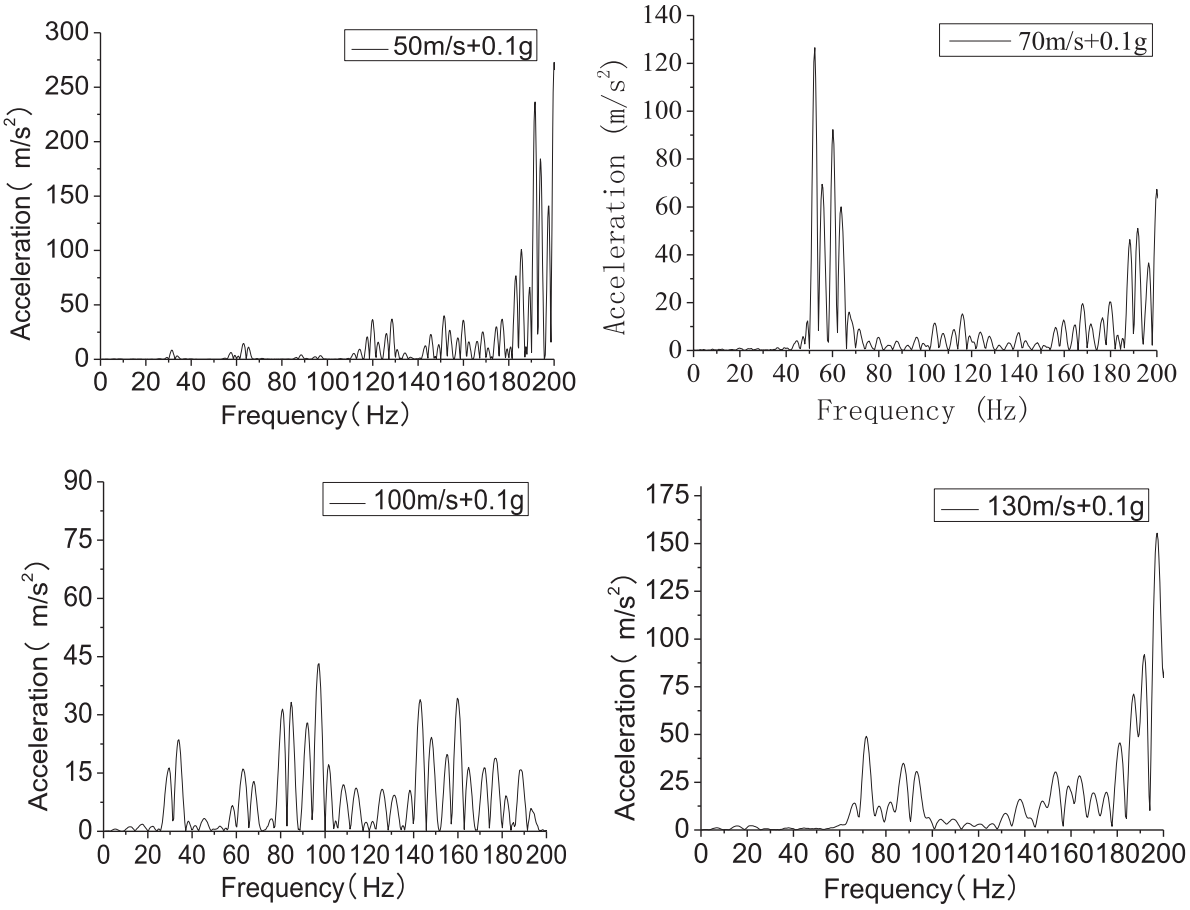

Fig. 23. Acceleration spectrum curve of composite load under different speed.

earthquake load. In this context, the vibration energy of the rail cannot be effectively propagated and attenuated, seriously affecting the comfort and safety of train operation.

5. Conclusions

The proposed track-subgrade-foundation interaction three-dimensional model is used to investigate the high-speed train-induced vibration (i.e. subgrade surface and rail structure) in the elastic soil. The comparison confirms a large difference in dynamic responses of these two different loading (i.e. single moving load and moving-earthquake composite load). Taking rail lateral deformation and derailment coefficient as important factors into consideration, the critical velocity of this model under train operation with or without seismic loading has been discussed. The major conclusions are summarized as follows.

1. Subjected to the action of earthquake-moving load, seismic load plays a leading role in the dynamic displacement of subgrade and rail, especially in the vertical positive displacement, which is likely to lead to train derailment.
2. The acceleration time history of subgrade and rail is sensitive to the change of train speed due to the composite loads. At critical speed, the peak value of subgrade acceleration reaches 10 m/s^2, and the acceleration amplitude of rail reaches 10^3m/s^2.
3. The derailment coefficient and the lateral displacement of the rail are taken as the indexes to evaluate the derailment of the train with respect to safety. When the lateral deformation and derailment coefficient of the train seriously exceed the standard, the vehicle is likely to lose stability or even derail, for example, at 50 m/s.
4. The critical speeds of 70 m/s (250 km/h) and 50 m/s (180 km/h) for subgrade and rail under composite load are found respectively, which are significantly smaller than the currently known critical speed of 350 km/h(99 ~ 105 m/s). Obviously, the critical speed due to moving-earthquake load is relatively low, which is easily exceeded by high-speed trains, thus inducing ground waves to cause strong vibration of track structures, eventually affecting the normal operation of trains and even derailing.

Acknowledgements

The research presented in this paper was supported by the Natural Science Foundation of China (No. 51808324) and Shandong Provincial Natural Science Foundation (No. ZR201702160391).

References

Bian, X.C., Chen, Y.M., Hu, T., 2008. Numerical simulation of high-speed train induced ground vibrations using 2.5D finite element approach. Sci. China-Phys. Mech. Astronomy 51 (6), 632–650.

Beskou, N.D., Tsinopoulos, S.V., Theodorakopoulos, D.D., 2016. Dynamic elastic analysis of 3-D flexible pavements under moving vehicles: A unified FEM treatment. Soil Dyn. Earthquake Eng. 82, 63–72.

Cai, Y.Q., Sun, H.L., Xu, C.J., 2008a. Three-dimensional analyses of dynamic responses of track-ground system subjected to a moving train load. Comput. Struct. 86 (7–8), 816–824.

Cai, Y.Q., Sun, H.L., Xu, C.J., 2008b. Response of railway track system on poroelastic half space soil medium subjected to a moving train load. Int. J. Solids Struct. 45 (18–19), 5015–5034.

Du, Y.Q., Bai, M.Z., Ni, S.R., 2014. Analysis of the subgrade dynamic stress under the trains opposite running on double-track high-speed railway. J. Beijing University Technol. 40 (4), 580–585 (in Chinese).

Eason, G., 1965. The stresses produced in a semi-infinite solid by a moving surface force. Int. J. Eng. Sci. 2, 581–609.

Feng, S.J., Zhang, X.L., Lei, W., et al., 2017. In situ experimental study on high speed train induced ground vibrations with the ballast-less track. Soil Dyn. Earthquake Eng. 102, 195–214.

Gao, G.Y., Xu, C.X., Chen, J., Song, J., 2018. Investigation of ground vibrations induced by trains moving on saturated transversely isotropic ground. Soil Dynamics and Earthquake Engineering. Soil Dyn. Earthquake Eng. 104, 40–44.

Gao, G.Y., Chen, J., Yang, J., Meng, Y., 2017. Field measurement and FE prediction of vibration reduction due to pile-raft foundation for high-tech workshop. Soil Dyn. Earthquake Eng. 101, 264–268.

Gao, G.Y., Li, N., Gu, X.Q., 2015. Field experiment and numerical study on active vibration isolation by horizontal blocks in layered ground under vertical loading. Soil Dyn. Earthquake Eng. 69, 251–261.

Gao, G.Y., Chen, Q.S., He, J.F., Liu, F., 2012. Investigation of ground vibration due to trains moving on saturated multi-layered ground by 2.5D finite element method. Soil Dyn. Earthquake Eng. 40, 87–98.

Hung, H.H., Chen, G.H., Yang, Y.B., 2013. Effect of railway roughness on soil vibrations due to moving trains by 2.5D finite/infinite element approach. Eng. Struct. 57, 254–266.

Yau, J.D., Frýba, L., 2007. Response of suspended beams due to moving loads and vertical seismic ground excitations. Eng. Struct. 29, 3255–3262.

Joyner, W.B., Boore, D.M., 1981. Peak horizontal acceleration and velocity from strong-motion records including records from the 1979 Imperial Valley, California, earthquake. Bull. Seismol. Soc. Am. 71 (6), 2011–2038.

Lefeuve-Mesgouez, G., Mesgouez, A., 2012. Three-dimensional dynamic response of a porous multilayered ground under moving loads of various distributions. Adv. Eng. Softw. 46 (1), 75–84.

Ministry of Construction of China. 2009. GB 50111-2006. Code for Seismic Design of Railway Engineering. Beijing: China Planning Press.

Ministry of Railways of China, 2009. TB 10621–2009, Code for Design of High-speed Railway. China Ministry of Railways Press, Beijing.

Paolucci, R., Maffeis, A., Scandella, L., Stupazzini, M., Vanini, M., 2003. Numerical prediction of low-frequency ground vibrations induced by high-speed trains at Ledsgaard, Sweden. Soil Dynamics Earthquake Eng. 22 (6), 425–433.

Fang, R., Zheng, Lu, Yao, H., Luo, X., Yang, M., 2018. Study on dynamic responses of unsaturated railway subgrade subjected to moving train load. Soil Dyn. Earthquake Eng. 115, 319–323.

Ruiz, J.F., Cost, P.A., Calçada, R.L.E., 2017. Medina, A. Colaçob. Study of ground vibrations induced by railway traffic in a 3D FEM model formulated in the time domain: experimental validation. Struct. Infrastruct. Eng. 13, 652–664.

Schnellboegl G. 2009. Early warning system for transport line. EWS Workshop, edilon-sedra GmbH, Munich, F. Quante.

Sheng, X., Jones, C.J.C., Thompson, D.J., 2004. A theoretical study on the influence of the track on train-induced ground vibration. J. Sound Vibration 272 (3–5), 909–936.

Song Xiao-lin, Zhai Wan-ming. 2012. Dynamic stress distribution of the infrastructure of CRTS II slab ballastless track under high speed moving load. China Railway Science.33 (4):1 -6. (in Chinese).

Sun, Z., Zhang, Y., Guo, D., Yang, G., Liu, Y., 2014. Research on Running Stability of CRH3 High Speed Trains Passing by Each Other. Eng. Appl. Computational Fluid Mechanics 8 (1), 140–157.

Takemiya, Hirokazu1. 2003. Simulation of track–ground vibrations due to a high-speed train: the case of X-2000 at Ledsgard. Journal of Sound and Vibration, 261(3): 503-526.

Tanabe, M., Matsumoto, N., Wakui, H., Sogabe, M., Okuda, H., Tanabe, Y., 2008. A simple and efficient numerical method for dynamic interaction analysis of a high-speed train and railway structure during an earthquake. J. Comput. Nonlinear Dyn. 3 (4) 041002.

Wang, M.Z., Cai, C.B., Zhu, S.Y., Zhai, W.M., 2016. Experimental study on dynamic performance of typical nonballasted track systems using a full-scale test rig. Proce. Institution Mechanical Engineers, Part F: J. Rail Rapid Transit 231 (4), 470–481.

Fu-chun, Xue, Jian-min, Zhang, 2014. Spatial distribution of vibration accelerations in coupled rail-embankment foundation system on high-speed railway under moving loads. Chinese Journal of Geotechnical Engineering 36 (12), 2179–2187 (in Chinese).

Yuan, Z.H., Cai, Y.Q., Cao, Z.G., 2016. An analytical model for vibration of a tunnel embedded in a saturated full-space to a harmonic point load. Soil Dyn. Earthquake Eng. 86 (6), 25–40.

Yao, H.L., Hu, Z., Lu, Z., Wang, H., 2016. Analytical model to predict dynamic responses of railway subgrade due to high-speed trains considering wheel–track interaction. Int. J. Geomech. 16 (2), 737–756.

Yi, S.R., 2018. Dynamic Analysis of High-Speed Railway Alignment. Southwest Jiao Tong University Press, 73–108.

Zeng, Z.P., Zhao, Y.G., Xu, W.T., Yu, Z.W., Chen, L.K., Lou, P., 2015. J. Sound Vib. 342, 22–43.

Zhai Wanming, He Zhenxing, Song Xiaolin. 2010. Prediction of high-speed train induced ground vibration based on train-track-ground system model. Earthquake Engineering and Engineering Vibration, 9 (04): 545-554.

Zhai Wanming, Wang Kaiyun, Cai Chengbiao. 2009. Fundamentals of Vehicle-track coupled dynamics, Vehicle System Dynamics: International Journal of Vehicle Mechanics and Mobility, 47(11): 1349-1376.

Zhang, N., Xia, H., Roeck, G.D., 2010. Dynamic analysis of train-bridge system under multi-support seismic excitations. J. Mech. Sci. Technol. 24, 2181–2188.

Zhuang, H.Y., Chen, G.X., Hu, Z.H., Qi, C.Z., 2016. Influence of soil liquefaction on the seismic response of a subway station in model tests. Bull. Eng. Geol. Environ. 75 (3), 1169–1182.